Document downloaded from:

http://hdl.handle.net/10251/143781

This paper must be cited as:

Wittee Lopes, C.; Cerrillo, JL.; Palomares Gimeno, AE.; Rey Garcia, F.; Agostini, G. (14-0). An in situ XAS study of the activation of precursor-dependent Pd nanoparticles. Physical Chemistry Chemical Physics. 20(18):12700-12709. https://doi.org/10.1039/C8CP00517F

The final publication is available at

https://doi.org/10.1039/C8CP00517F

Copyright The Royal Society of Chemistry

Additional Information

Check for updates

View Article Online
View Journal

PCCP

Accepted Manuscript

This article can be cited before page numbers have been issued, to do this please use: C. W. Lopes, J. L. Cerrillo, E. Palomares, F. Rey and G. Agostini, *Phys. Chem. Chem. Phys.*, 2018, DOI: 10.1039/C8CP00517F.

This is an Accepted Manuscript, which has been through the Royal Society of Chemistry peer review process and has been accepted for publication.

Accepted Manuscripts are published online shortly after acceptance, before technical editing, formatting and proof reading. Using this free service, authors can make their results available to the community, in citable form, before we publish the edited article. We will replace this Accepted Manuscript with the edited and formatted Advance Article as soon as it is available.

You can find more information about Accepted Manuscripts in the author guidelines.

Please note that technical editing may introduce minor changes to the text and/or graphics, which may alter content. The journal's standard Terms & Conditions and the ethical guidelines, outlined in our author and reviewer resource centre, still apply. In no event shall the Royal Society of Chemistry be held responsible for any errors or omissions in this Accepted Manuscript or any consequences arising from the use of any information it contains.

View Article Online
DOI: 10.1039/C8CP00517F

An *in situ* XAS study of the activation of precursor-dependent Pd nanoparticles

Christian W. Lopes[ab], *Jose L. Cerrillo*[a], *Antonio E. Palomares*[a], *Fernando Rey*[a], *Giovanni Agostini*[c*]

[a]Instituto de Tecnología Química (Universitat Politècnica de València – Consejo Superior de Investigaciones Científicas), Avda. de Los Naranjos s/n, Valencia 46022, Spain.
[b]CAPES Foundation, Ministry of Education of Brazil, Brasília 70040-020, Brazil.
[c]Leibniz-Institut für Katalyse, Albert-Einstein-Straβe 29a, Rostock 18059, Germany.
Email: Giovanni.Agostini@catalysis.de

Published on 05 April 2018. Downloaded by Freie Universitaet Berlin on 06/04/2018 12:02:04.

Physical Chemistry Chemical Physics Accepted Manuscript

†Electronic supplementary information (ESI) available

View Article Online
DOI: 10.1039/C8CP00517F

Published on 05 April 2018. Downloaded by Freie Universitaet Berlin on 06/04/2018 12:02:04.

Abstract

The activation of precursor-dependent Pd nanoparticles was comprehensively followed by *in situ* X-ray absorption spectroscopy on two inorganic supports for rationalizing the final catalytic activity. Two series of Pd-based catalysts (7 wt% Pd) were prepared by impregnation of γ-Al_2O_3 and activated carbon supports varying the metal precursor ($Pd(NO_3)_2$, $PdCl_2$ and $Pd(OAc)_2$). The most relevant physicochemical properties of studied catalysts were determined by several techniques including ICP-OES, XRD, N_2 adsorption and XAS. The results indicate that the thermal stability of metal precursors plays an important role on the size and speciation of formed Pd nanoparticles after activation process. The Cl-based precursor, which presents high thermal stability, passes through a PdO_xCl_y mixed phase when submitted to calcination on Pd/Al_2O_3 and leaves Cl-species after metal reduction on Pd/C (which can be detrimental to catalytic reactions). Differently, $Pd(OAc)_2$ and $Pd(NO_3)_2$ promotes the formation of larger species due to different precursor decomposition pathway. Ordered PdO is observed even before calcination when $Pd(NO_3)_2$ was used as metallic source, which translates into large nanoparticles after reduction in H_2. By using average coordination numbers of Pd species obtained from EXAFS data of as-reduced catalysts, a correlation was observed comparing the three precursors: the $PdCl_2$ generates smaller nanoparticles than $Pd(OAc)_2$, which in turn generates smaller nanoparticles than $Pd(NO_3)_2$, regardless of the support used for catalyst preparation.

Keywords: Pd nanoparticles; *in situ*; XANES; EXAFS; X-ray Absorption Spectroscopy

Physical Chemistry Chemical Physics Accepted Manuscript

View Article Online
DOI: 10.1039/C8CP00517F

Published on 05 April 2018. Downloaded by Freie Universitaet Berlin on 06/04/2018 12:02:04.

Physical Chemistry Chemical Physics Accepted Manuscript

INTRODUCTION

Palladium-based catalysts are used since many years as selective heterogeneous catalysts for hydrogenation reactions in different industrial processes, from petrochemical to the synthesis of fine and bulk chemicals and removal of water pollutants.[1-9] Since palladium is one of the rarest elements available on earth, the European Community has recently included this metal in the list of raw materials deemed critical in terms of supply risk.[10] Because of this, the control of the synthesis parameters of Pd-based catalysts, such as: metal precursor, activation method, type of support, should be evaluated for tuning the catalysts properties in order to ultimately impact the catalytic performance. On this optimization, proper characterization of the Pd-catalysts is a key stone for increasing catalytic activity and selectivity, while reducing the required amount of noble metal.

Among the variables that influence the catalyst activity, the study of metallic precursor is important due to the different decomposition pathway/kinetic of the precursor during catalyst activation processes (calcination/reduction).[11, 12] Indeed, the nature of Pd precursor can determine the final properties of the metal nanoparticle, such as particle size and remaining undecomposed species, which could poison the catalysts.[13] A second important parameter is the type of the activation process, which influences the final activity of the Pd-based hydrogenation catalysts. Also, the transformation *precursor to nanoparticle* can be dictated by the type of support due to its different thermal and chemical properties.[11] Therefore, systematic investigation that makes possible the characterization of complex and disordered nanoparticle systems capable to track information at different catalysts activation steps is essential for understanding the final catalytic performance of the Pd-based catalyst.

Currently, X-ray absorption spectroscopy is one of the most powerful tools for characterization of metal nanoparticles, due to its element-selective character, making possible the *in situ* follow-up of changes resulting from activation treatments, as already observed in literature.[14-17] Performing linear combinations, mixed phases can be characterized, since XANES features are considered the fingerprint of phases present in the sample.[18] Also, by analyzing the EXAFS region (either looking at the imaginary or real part of Fourier transform), the absorber neighbors with different scattering ($Z > 1$) can be discriminated, helping in the understanding of

View Article Online
DOI: 10.1039/C8CP00517F

Published on 05 April 2018. Downloaded by Freie Universitaet Berlin on 06/04/2018 12:02:04.

Physical Chemistry Chemical Physics Accepted Manuscript

complex systems which cannot be characterized by other techniques due to the lack of order of these compounds. Moreover, with development of methods for data analysis/interpretation, it is possible to estimate nanoparticle size, shape and disorder in the nm range by different approaches.[19-22] The combination of characterization techniques is being used to rationalize particle size distribution interpretations, using EXAFS as a core technique.[23]

In the present work, we have studied the influence of the metal precursor on the formation of Pd species on two series of catalysts, using two types of widely employed[11] and cheap supports with different textural and chemical/thermal properties (activated carbon and γ-alumina). To do that, a comprehensive study by *in situ* X-ray absorption spectroscopy has been performed during catalysts activation (as-prepared/calcination/reduction), trying to follow the evolution and changes in the physicochemical properties (oxidation state, size of metal formed species) of the catalysts and the difference among them for further structure-reactivity relationships. Furthermore, an elegant approach has been used to determinate the fraction of oxidized Pd and undecomposed precursor, when the XAS spectrum is formed by both types of species. Finally, the consequences of different activation procedures have been discussed in terms of average coordination number obtained from EXAFS co-refinement fits. To the best of our knowledge, this is the first report in which the influence of the metal precursor and effect of the support have been embraced studied by an in situ XAS spectroscopy during catalyst activation.

EXPERIMENTAL METHODS

Catalysts preparation

The Pd-based catalysts (7 wt%) have been prepared by impregnation and drying method [12] varying Pd precursors: $Pd(OAc)_2$, $PdCl_2$ and $Pd(NO_3)_2$. The support, γ-Al_2O_3 (Merck) or granular activated carbon (Norit GAC 1240W), was dispersed in an aqueous solution of Pd precursor (containing the intended amount of Pd), with a liquid to solid ratio of 5. The mixture was rotaevaporated until dryness, resulting in a sample that contains the carrier and the studied precursor (as-prepared). In the case of $PdCl_2$, some drops of HCl were added to the solution for increasing the solubility of precursor in water[11]. Afterwards, the catalysts were dried at 100 ºC for 1 hr and stored before calcination/reduction treatments. The prepared catalysts are labeled as

View Article Online
DOI: 10.1039/C8CP00517F

Published on 05 April 2018. Downloaded by Freie Universitaet Berlin on 06/04/2018 12:02:04.

PdX-Y, where X stands for Al_2O_3 (Al) or activated carbon (C); and Y refers to the Pd precursor, i.e., palladium nitrate (NO_3), palladium chloride (Cl) or palladium acetate (Ac).

All these catalysts have been selected because their very high activity for selective reduction of bromates in water. Indeed, all of them reach 100 % conversion at room temperature after a few minutes of reaction in batch condition (0.5g catalyst, 600 mL of a solution with 50 ppm of potassium bromate and 250 mL $H_2 \cdot min^{-1}$) (a detailed catalytic discussion will be published elsewhere).

Characterization techniques

The Pd content of catalysts supported on γ-Al_2O_3 was determined by ICP-OES in a Varian 715-ES after dissolution of the powder samples (approx. 20-30 mg) in 5 ml of an acid mixture of 20%HNO_3:20%HF:60%HCl (% volume). After complete solution of the samples, distilled water was added until 60 ml. The metal content of catalysts supported on activated carbon was not possible to be measured by ICP-OES using the digestion method applied for alumina-based catalysts. Then, the Pd contents of the carbon-based catalysts were estimated from their Pd-*edge jump* in XANES region. Thermogravimetric analyses of Pd precursors were performed in an alumina pan with a Mettler Toledo TGA/SDTA 851e flowing O_2 from ambient to 800 ºC at a heating rate of 10 ºC$\cdot min^{-1}$. Phase identification was performed by powder-XRD using a Philips Cubix-Pro X'Pert diffractometer, operating at 45 kV and 40 mA, and using Cu Kα radiation (λ = 1.542 Å). The experimental XRD patterns were compared with crystallographic JCPDS standards of PdO (00-006-0515), γ-Al_2O_3 (00-010-0425) and $AlCl_3 \cdot 6H_2O$ (00-008-0453). Textural properties were determined from the N_2 adsorption isotherms measured at −196 ºC in an ASAP-2420 equipment (Micromeritics). Prior to the N_2 adsorption measurements, the samples were degassed at 400 ºC (for γ-Al_2O_3) and 200 ºC (for activated carbon) overnight. Specific surface areas (S_{BET}) were obtained using the BET (Brunauer-Emmett-Teller) method[24] at relative pressures (p/p^0) ranging from 0.05 to 0.1 and 0.02 to 0.09 for catalysts based on alumina and carbon, respectively. The micropore volume for Pd/C catalysts was derived from t-plot method[25] at relative pressures (p/p^0) ranging from 0.39 to 0.64. The total pore volumes were determined using the Gurvich rule at p/p^0 of 0.97[26]. The Pd

Physical Chemistry Chemical Physics Accepted Manuscript

View Article Online
DOI: 10.1039/C8CP00517F

Published on 05 April 2018. Downloaded by Freie Universitaet Berlin on 06/04/2018 12:02:04.

nanoparticles formed on alumina and carbon supports were studied by transmission electron microscopy (TEM) using a JEOL 2100F microscope operating at 200 kV. The sample powders were ultrasonically dispersed in isopropanol and transferred to a holey-carbon coated copper grid. The magnification was selected for each sample to obtain a relatively large statistic with enough size resolution.

X-ray absorption experiments, at the Pd K-edge (24350 eV), were performed at the BL22 (CLÆSS) beamline of ALBA synchrotron (Cerdanyolla del Vallès, Spain)[27]. The white beam was monochromatized using a Si (311) double crystal; harmonic rejection has been performed using Rh-coated silicon mirrors. The spectra were collected in transmission mode by means of the ionization chambers. Samples in the form of self-supported pellets of optimized thickness for an edge jump about 1 have been located inside the multipurpose *in situ* cell described by Guilera[28]. Energy calibration was checked by Pd foil placed between second and third ionization chamber.

Activation process was followed at different steps (**Fig. S1** exemplifies the whole procedure, ESI†): i) the spectra were collected starting from room temperature (25 ºC) up to 500 ºC at 10 ºC·min^{-1} under O_2 flow (20% O_2/He) in the calcination process and cooled down to room temperature. ii) Then, the temperature is raised to 200 ºC at 10 ºC·min^{-1} under hydrogen flow (5% H_2/He - reduction process) and then it is cooled down to room temperature. The carbon-based samples were only submitted to the reduction step because carbon may suffer surface oxidation during calcination and then, modifying the physicochemical properties of the final catalysts. At least, three scans were acquired at each measurement step to ensure spectral reproducibility and good signal-to-noise ratio. Data reduction and extraction of the χ(k) signal has been performed using Athena code[29]. EXAFS data analysis has been performed using the Arthemis software[29], phase and amplitudes have been calculated by FEFF6 code.

RESULTS AND DISCUSSION

Characterization of supports and Pd-based catalysts

The different crystalline phases occurring on the samples were investigated by XRD. The X-ray patterns of Al_2O_3 supported catalysts (in their oxidized state), shown in **Fig. 1a**, are

Physical Chemistry Chemical Physics Accepted Manuscript

View Article Online
DOI: 10.1039/C8CP00517F

Published on 05 April 2018. Downloaded by Freie Universitaet Berlin on 06/04/2018 12:02:04.

dominated by reflections of γ-Al_2O_3. There is a clear diminution of the characteristic peaks of alumina upon Pd incorporation in the PdAl-Cl catalysts, which is attributed to the loss of ordering and to the formation of $AlCl_3 \cdot 6H_2O$ during Pd impregnation with $PdCl_2$ + HCl (used for $PdCl_2$ solubilization). This is also confirmed by the appearance of a peak at 27º assigned to $AlCl_3 \cdot 6H_2O$ in the XRD pattern of PdAl-Cl sample. In addition to alumina peaks, PdAl-NO_3 sample exhibit broad reflections at 33.8, 54.8 and 71º assigned to PdO phase .[30] The intensities of the PdO peaks are more evident in PdAl-NO_3 than in other catalysts, due to the ease decomposition of $Pd(NO_3)_2$ with temperature, which consequently results in the formation of PdO during impregnation step.

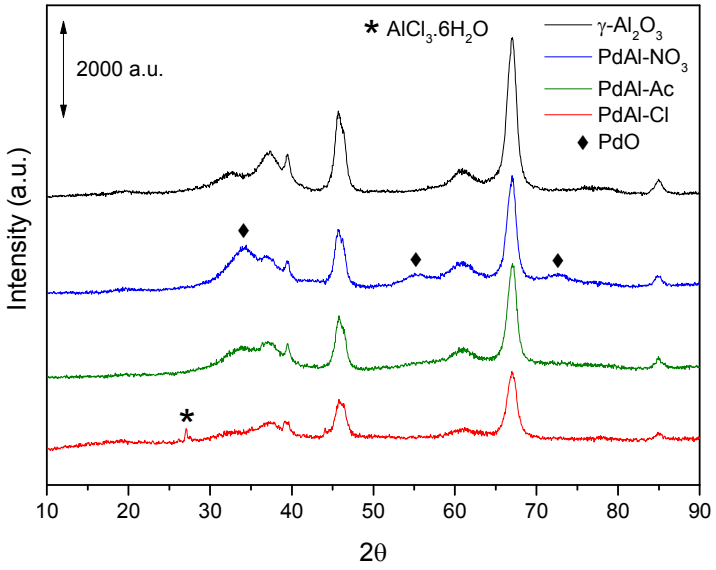

Fig. 1 X-ray diffraction patterns of the as-made Pd-supported on γ-Al_2O_3.

N_2 adsorption isotherms (**Fig. 2**) for the Pd-based catalysts and supports were performed and the derived textural properties are summarized in **Table 1**. Catalysts based on γ-Al_2O_3 (**Fig. 2a**) present Type III isotherms, characteristic of non-porous or macroporous solids. In this case, the isotherms do not present Point B and consequently no identifiable monolayer generation Moreover, most of amount adsorbed remain close to saturation pressure (i.e., at $p/p^0 = 1$)[31]. As γ-Al_2O_3 used in this work does not present microporosity, the contribution of micropores to S_{BET} is negligible. Conversely, the catalysts based on activated carbon (**Fig. 2b**) show Type I isotherms, which are given by microporous solids having relatively small external surfaces. The abrupt increase in quantity adsorbed at very low p/p^0 is due to enhanced adsorbent-adsorptive

Physical Chemistry Chemical Physics Accepted Manuscript

View Article Online
DOI: 10.1039/C8CP00517F

Published on 05 April 2018. Downloaded by Freie Universitaet Berlin on 06/04/2018 12:02:04.

interactions in narrow micropores of molecular dimensions, resulting in the filling of these pores at very low p/p^0. Recently IUPAC has discriminated between two Type I isotherms[29], samples having ultramicroporosity (Type I(a)) and solids with conventional microporosity (Type I(b)). In this study, the samples can be classified as Type I(b), typical of materials with pore size distributions over a broader range including relatively large micropores and possibly overlapping in the region of narrow mesopores (< 2.5 nm)[31].

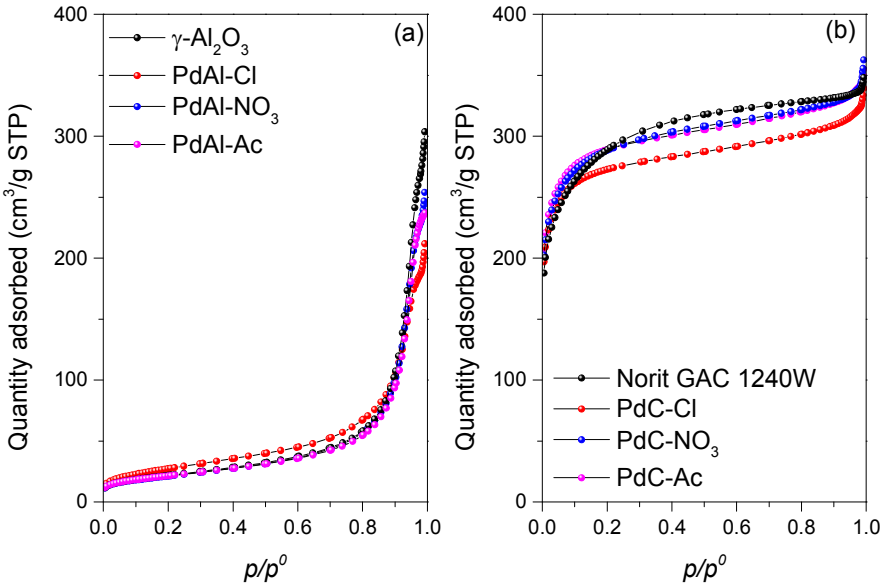

Fig. 2 N_2 adsorption isotherms for the activated Pd-supported on γ-Al_2O_3 (a) and activated carbon (b) catalysts as well as their supports.

The PdAl-Cl catalyst presents a slightly higher surface area (97 m^2/g) and decreased total pore volume (TPV) value (0.28 cm^3/g) among the studied catalysts using γ-Al_2O_3 as support, which can be explained by the partially modification of support (as seen by XRD) suffered by the highly acidic media during metal impregnation. PdAl-Ac and PdAl-NO_3 catalysts present roughly the same textural properties in comparison with γ-Al_2O_3, demonstrating that metal impregnation does not affect the porosity of the alumina support. Textural properties of carbon-based Pd catalysts remains essentially unchanged with respect to the original activated carbon as it is shown in **Table 1**, regardless the nature of the Pd precursor used for the catalyst preparation,

The Pd content of the catalysts measured by ICP-OES is shown in **Table 1**. The concentration of Pd in the catalysts supported on alumina is in good agreement with the targeted

Physical Chemistry Chemical Physics Accepted Manuscript

View Article Online
DOI: 10.1039/C8CP00517F

Published on 05 April 2018. Downloaded by Freie Universitaet Berlin on 06/04/2018 12:02:04.

value (7 wt%), with minor deviations between 0.1-0.2% for PdAl-Ac (6.9 wt%) and PdAl-Cl (7.2 wt%). On the other hand, it was not possible to determinate the Pd content by ICP-OES on carbon-based samples, because of the insolubility of carbon in the acid mixture used for the measurement. However, the edge jump obtained in the XAS measurements is consistent with a metal loading of 7 wt%.

Table 1 Chemical composition and textural properties of supports and Pd-based catalysts.

Sample	wt% Pd	S_{BET} (m^2/g)	Vμ (cm^3/g)	TPV (cm^3/g)
γ-Al_2O_3	-	77	0	0.40
PdAl-Ac	6.9	76	0	0.35
PdAl-Cl	7.2	97	0	0.28
PdAl-NO_3	7.0	75	0	0.35
Activated carbon	-	1068	0.44	0.52
PdC-Ac	~ 7*	1109	0.42	0.52
PdC-Cl	~ 7*	1050	0.39	0.50
PdC-NO_3	~ 7*	1094	0.42	0.52

* Pd content estimated from the Pd K-edge jump in the XANES region.

TEM investigation performed on samples after reduction process shows the formation of Pd particles in the nanometer range, selected images are reported in **Fig. S6** (ESI†).

Characterization of activation process of catalysts by XAS

In order to allow correct interpretation a set of reference compounds (Pd foil, PdO, $Pd(NO_3)_2$, $Pd(OAc)_2$, $PdCl_2$) were measured under ambient conditions and used as standards. **Fig. 3** exhibits the XANES spectra (a) and k^3-weighted (phase-uncorrected) |FT| (b) of Pd standards with oxidation state 2+ and 0. All patterns have been chosen considering possible Pd local environments that could be present during the activation step of catalysts. The absorption edge feature for Pd metal at 24350 eV (better seen in first-derivative, inset of **Fig. 3a**) is due 1s to 4d dipole forbidden transition according to the selection rules, Δl=1 and Δj=1, where l and j are the orbital angular momentum and the total angular momentum of the local density of states, respectively[32]. The first oscillations of Pd metal appears immediately after the edge, positioned at 24367 and 24391 eV, referent to 1s→5p and 1s→4f electronic transitions[32], respectively. These two strong features are due to the well-arranged local *fcc* structure, where 12 Pd atoms are

Physical Chemistry Chemical Physics Accepted Manuscript

View Article Online
DOI: 10.1039/C8CP00517F

Published on 05 April 2018. Downloaded by Freie Universitaet Berlin on 06/04/2018 12:02:04.

coordinated at the same distance from the central Pd atom[33]. Therefore, the intensity of these features contains intrinsically information on the Pd particle size. When the size of Pd metal particles is small, there is a large fraction of low coordinated atoms, causing low amplitude of the EXAFS oscillation[32]. Features in the pre-edge region are not observed in any spectra of patterns, which suggest centrosymmetric geometry around palladium atoms in any temperature/atmosphere studied (which will be the case of all studied catalysts in this paper)[34]. For compounds with oxidation state 2+, such as PdO, $PdCl_2$, $Pd(OAc)_2$ and $Pd(NO_3)_2$ the energy threshold appears at 24354 eV. When a d-p orbital hybridization take place, as for Pd^{2+} compounds, a significantly strong absorption cross-section can be seen, compared with that of Pd foil[32]. The position and intensity of the peaks in the |FT| (**Fig. 3b**) reflect the coordination and the distances around metal. The PdO, $Pd(OAc)_2$ and $Pd(NO_3)_2$ show the first coordination shell at the same position (~1.5 Å) in the k^3-weighted (phase-uncorrected) |FT|, characteristic of Pd-O bond in square-planar compounds. With the exception of PdO, which contains a significant contribution between 2-4 Å (red spectrum) due to higher shells,[35] the higher shells of $Pd(OAc)_2$ and $Pd(NO_3)_2$ are not easily visible and it is hard to discriminate even looking at the imaginary part of the |FT| (inset of **Fig. 3b**). Unlike the oxygen-based standards, the $PdCl_2$ and Pd metal first shells lie at longer distances (1.88 Å for $PdCl_2$ and 2.5 Å for Pd^0, respectively) and are much more intense (15-20 $Å^{-4}$ in intensity) due to the presence of heavier atoms and/or in more quantity (e.g. 12 Pd first-neighbors in Pd metal). In case of overlapping of mixed phases (close R-values in |FT|), the imaginary part of Fourier transform is very informative and can help in the EXAFS data interpretation, in particular, PdO and $PdCl_2$ exhibit the minimum position of first contribution at 1.580 and 1.696 Å, respectively. Nonetheless, the first shell in Pd^0 and second and third shells of PdO are composed by Pd-Pd contributions and can be differentiated in the Imm of |FT| using the minimum at 2.79 and maximum at 2.97 Å of PdO which are not present in Pd metal spectrum.

Physical Chemistry Chemical Physics Accepted Manuscript

View Article Online
DOI: 10.1039/C8CP00517F

Published on 05 April 2018. Downloaded by Freie Universitaet Berlin on 06/04/2018 12:02:04.

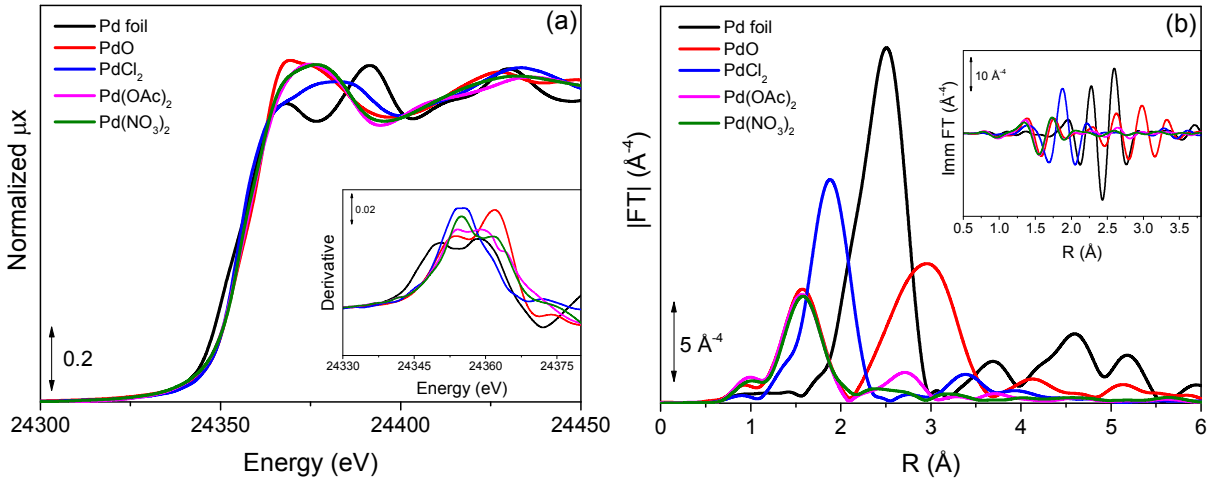

Fig. 3 Normalized XANES spectra (a) and |FT| of the k^3-weighted $\chi(k)$ functions (b) of Pd standards. The inset in part (a) shows the derivatives of the normalized XANES spectra and in (b) shows the imaginary parts of the FT of the k^3-weighted $\chi(k)$ functions for Pd standards.

The quantitative results derived from EXAFS data analysis of Pd standards are shown in **Table S1** (ESI†). For all optimized compounds, only the first coordination sphere was fitted using a specific R-range for each studied standard, depending on the distance of Pd-ligand path. For Pd metal foil, a characteristic coordination number of 12 is fixed according to bulk value and the Pd-Pd distance of 2.74 Å was obtained, typical of noble metals arranged in *fcc* local structure. The other standards exhibit coordination number of 4, typical of palladium compounds in oxidation state 2+ in square-planar geometry,[11, 36] with distances Pd-O of 2.02 and 2.00 Å for PdO and $Pd(OAc)_2$, respectively, and a distance Pd-Cl of 2.31 Å for $PdCl_2$, in accordance with crystallographic data of these compounds. All studied standards show a Debye-Waller factor typical of well-ordered materials[37].

The state of Pd in the catalysts was evaluated in different stages of the activation process and the normalized XANES spectra and k^3-weighted (phase-uncorrected) |FT| of the as-prepared samples are represented in **Fig. 4a**.

Physical Chemistry Chemical Physics Accepted Manuscript

View Article Online
DOI: 10.1039/C8CP00517F

Published on 05 April 2018. Downloaded by Freie Universitaet Berlin on 06/04/2018 12:02:04.

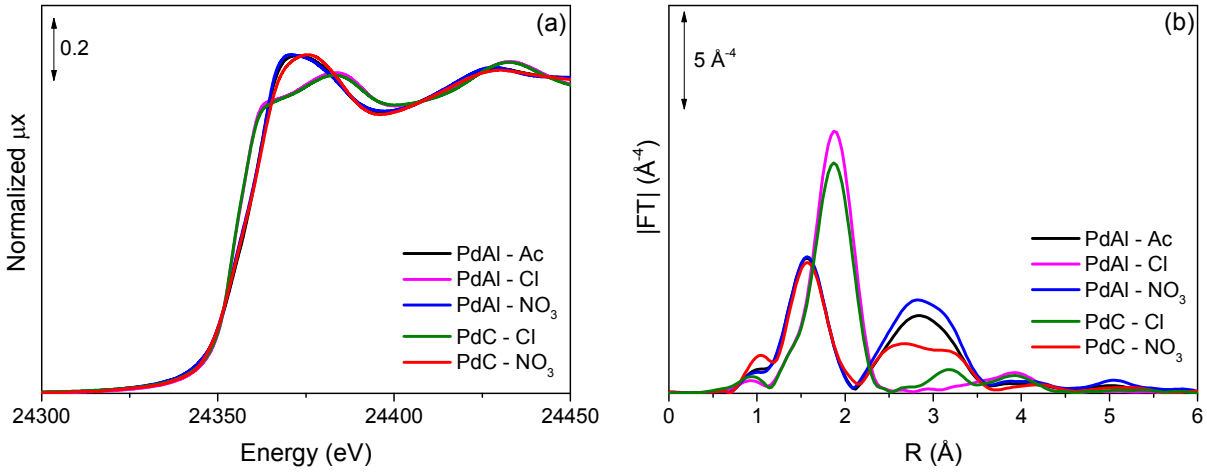

Fig. 4 Normalized XANES spectra (a) and |FT| of the k^3-weighted χ(k) functions (b) of the as-prepared catalysts (before activation process).

All XANES of the as-prepared catalysts collected before calcination show the absorption edge positioned at 24354 eV, characteristic of Pd in oxidation state 2+. PdAl-Ac and PdAl-NO_3 spectra collected in air at room temperature are almost overlapped to PdO, indicating an easily decomposition of Pd precursor during the impregnation/drying step with consequently formation of PdO, which is in agreement with XRD data. For PdAl-Cl the spectrum of sample at starting point is different from PdO and attributed to $PdCl_2$, suggesting that $PdCl_2$ is not decomposed as well as others during impregnation/drying step of catalyst preparation. As observed in the thermogravimetric curves of **Fig. S2** (ESI†), the $Pd(NO_3)_2$ is decomposed at much lower temperature than $PdCl_2$, starting from 90 ºC with temperature of maximum reaction rate at 140 ºC while $PdCl_2$ decomposition starts at >500 ºC. Otherwise, the $Pd(OAc)_2$ decomposition takes place in an intermediate temperature between $Pd(NO_3)_2$ and $PdCl_2$. Both catalysts based on palladium chloride exhibit the typical EXAFS spectra (**Fig. 4b**) of $PdCl_2$ without pronounced contribution for higher shells, indicating a good dispersion of precursor over the support. The other three EXAFS spectra of catalysts containing PdO after impregnation (PdAl-Ac, PdAl-NO_3, PdC-NO_3) exhibit the same features although with almost double intensities of contributions from 2th and 3th shells (2.0-3.5 Å) for Al_2O_3-based compared to C-based, which point out the higher degree of crystallinity of formed PdO in Pd/Al_2O_3 catalyts.

The quantitative results derived from EXAFS data analysis of as-prepared Pd catalysts are reported in **Table 2**. Most catalysts present the expected average coordination number of

Physical Chemistry Chemical Physics Accepted Manuscript

View Article Online
DOI: 10.1039/C8CP00517F

Published on 05 April 2018. Downloaded by Freie Universitaet Berlin on 06/04/2018 12:02:04.

approximately 4 and all catalysts in their as-prepared state presented main parameters in accordance with crystallographic data and EXAFS of respective studied precursors.

Table 2 Summary of optimized parameters by fitting EXAFS data of as-prepared catalysts at 25 ºC in O_2[a]

Sample	CN	Path	R (Å)	σ^2 (Å^2)	ΔE_0 (eV)	r-factor
PdAl-Ac	4.0 ± 0.5	Pd-O	2.028 ± 0.006	0.0033 ± 0.0008	1.5 ± 1.8	0.0077
PdAl-Cl[b]	3.7 ± 0.1	Pd-Cl	2.311 ± 0.002	0.0034 ± 0.0002	4.3 ± 0.5	0.0009
PdAl-NO_3	4.2 ± 0.5	Pd-O	2.030 ± 0.006	0.0034 ± 0.0008	0.2 ± 1.7	0.0068
PdC-Cl[b]	3.6 ± 0.1	Pd-Cl	2.308 ± 0.002	0.0040 ± 0.0002	4.3 ± 0.4	0.0007
PdC-NO_3	3.9 ± 0.8	Pd-O	2.023 ± 0.011	0.0039 ± 0.0015	2.1 ± 2.9	0.0185

[a]The fits were performed on the first coordination shell (ΔR = 1.0-2.0 Å) over FT of the k^3-weighted χ(k) functions performed in the Δk = 2.3-13.7 Å^{-1} interval, resulting into a number of independent parameters of $2\Delta R\Delta k/\pi$ = 7.0. Non optimized parameters are recognizable by the absence of the corresponding error bar. [b]ΔR = 1.4-2.4 Å.

Once the PdO phase is already detected at room temperature in the catalysts derived from oxygen-based precursors, no substantially changes were expected in the XANES during calcination. The position of the edge (24354 eV – related to Pd^{2+}) is maintained constant during whole calcination step (RT → 500 ºC) without changes in XANES oscillations for the catalysts based on alumina and prepared using palladium nitrate and acetate. On the other hand, we expected changes in XANES features during decomposition process of $PdCl_2$ on PdAl-Cl catalyst. The calcination was followed and it is possible to observe an evolution in the XANES spectra (**Fig. 5a**) from that typical of $PdCl_2$ at 25 ºC to an intermediate (possibly PdO_xCl_y[38] mixed phase) spectrum that does not resembles PdO in the end of thermal treatment. Two main isosbestic points (A and B) positioned at 24363 and 24381 eV, respectively, can be seen. As already stated above, $PdCl_2$ is difficult to decompose, which makes it a complicated candidate in catalyst preparation when the final phase needs to be surface clean (without rests of precursor). The k^3-weighted (phase-uncorrected) |FT| are represented in **Fig. 5b**. The sample presents essentially one peak in |FT| during whole calcination process, attributed to the contribution Pd-Cl. With increasing temperature, the peak becomes flattened and a shoulder appears to the left (marked with an arrow), being this displacement an indicative of formation of a mixed PdO_xCl_y compound. Another possible route of decomposition could be the formation of the segregate $PdCl_2$ and PdO phases. The use of features (maxima and minima) of imaginary part of |FT| to obtain subtle information about metal systems is already known through literature[39]. In order to

Physical Chemistry Chemical Physics Accepted Manuscript

View Article Online
DOI: 10.1039/C8CP00517F

Published on 05 April 2018. Downloaded by Freie Universitaet Berlin on 06/04/2018 12:02:04.

find the proportion of PdO and $PdCl_2$ present in the catalyst in the end of calcination we have used the position of the feature *a* present in the imaginary parts of |FT| of spectra collected during calcination (inset of **Fig. 5b**) as fingerprint for PdO fraction (*b* value) and the results are expressed in **Table 3**. At 25 ºC, the feature *a* lies at 1.684 Å, closely related to the position obtained for $PdCl_2$ (1.696 Å) and as the temperature increases the position of *a* shifts to lower R (related to higher PdO fraction) values until reaching 1.608 Å at 500 ºC, showing also in this case two isosbestic points and giving rise to the formation of a $PdO_{0.75}Cl_{0.25}$ compound.

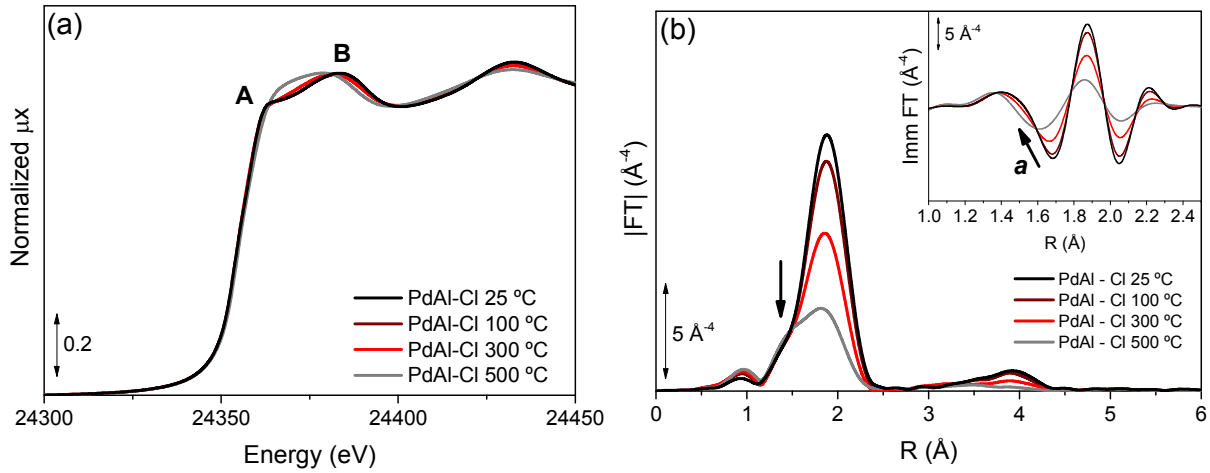

Fig. 5 Normalized XANES spectra (a) and |FT| of the k^3-weighted χ(k) functions (b) of PdAl-Cl sample during calcination. The inset in part (b) shows the imaginary parts of the FT of the k^3-weighted χ(k) functions of the sample during calcination.

Table 3 Correlation between the position of feature *a* in the imaginary parts of the FT of the k^3-weighted χ(k) functions and the fraction of PdO (*b*) in the PdAl-Cl sample at different steps of calcination.

Sample	**T (ºC)**	***a* Position**[b] **(Å)**	***PdO* Fraction *(b)* (%)**[a]
PdO	-	1.580	1
$PdCl_2$	-	1.696	0
PdAl-Cl	25	1.684	0.10
	100	1.680	0.13
	300	1.667	0.25
	500	1.608	0.75

[a]Calculated according PdO fraction *(b)* = (1.696-a)/1.580-1.696

[b] minimum position is obtained by fitting the Imaginary part of FT

Physical Chemistry Chemical Physics Accepted Manuscript

View Article Online
DOI: 10.1039/C8CP00517F

Published on 05 April 2018. Downloaded by Freie Universitaet Berlin on 06/04/2018 12:02:04.

After calcination the catalysts based on Al_2O_3 and carbon (not submitted to calcination) were treated in H_2 and the normalized XANES spectra collected at 25 ºC are shown in **Fig. 6a**. When the atmosphere is changed to hydrogen, the edge in Pd/Al_2O_3 catalysts is shifted to 24350 eV already at room temperature, indicating an easy reduction of Pd^{2+} species to Pd^0. Also, the first oscillations beyond the edge are flattened respect to foil, indicating a large fraction of low coordinated Pd atoms. It is also worth noticing that the oscillations beyond edge are slightly shifted 3 eV to the left respect to spectrum of Pd metal foil, which can be explained by the formation of PdH_x.[40, 41] The Pd/C catalysts maintain the edge position characteristic of Pd^{2+} (24354 eV) and only small modifications on the shape of XANES spectra are appreciated. This behavior could be associated to the presence of ligands avoiding the easy reduction observed in Pd/Al_2O_3 catalysts. In the moduli of Fourier transform (**Fig. 6b**) a small decreasing in intensity of 2.5 $Å^{-4}$ in the first shell for PdC-Ac indicates that a decomposition process of palladium acetate precursor takes place. In fact, the CN for Pd-O contribution in the first shell of $Pd(OAc)_2$ is 4 while for PdC-Ac is 1.9, corresponding to the loss of ligands due the reduction step ($Pd(OAc)_2 \rightarrow Pd^0$). For this catalyst, a higher Debye-Waller factor (0.0052 $Å^2$) has been observed in comparison with other samples, possibly due to a disorder effect with respect to decomposition process of precursor. Moreover, no changes in the other Pd/C samples are appreciate. Conversely, as stated by XANES, the three samples of Pd/Al_2O_3 change completely the profile, with the disappearing of features related to PdO and $PdCl_2$ and consequently nanoparticle formation is observed by the appearance of metallic palladium features. The differences in the size of Pd domains among the three Al_2O_3-based catalysts are observed, with slightly different intensity of Pd first shell for PdAl-Ac and PdAl-NO_3 being roughly four times more intense than this contribution in PdAl-Cl. Also, comparing the reduced samples with Pd foil, a shift of ~0.1 Å to higher R-values in the whole spectrum position (first and higher shells) is observed, which can be attributed to the formation of PdH_x also visible in XANES spectra.

Physical Chemistry Chemical Physics Accepted Manuscript

View Article Online
DOI: 10.1039/C8CP00517F

Published on 05 April 2018. Downloaded by Freie Universitaet Berlin on 06/04/2018 12:02:04.

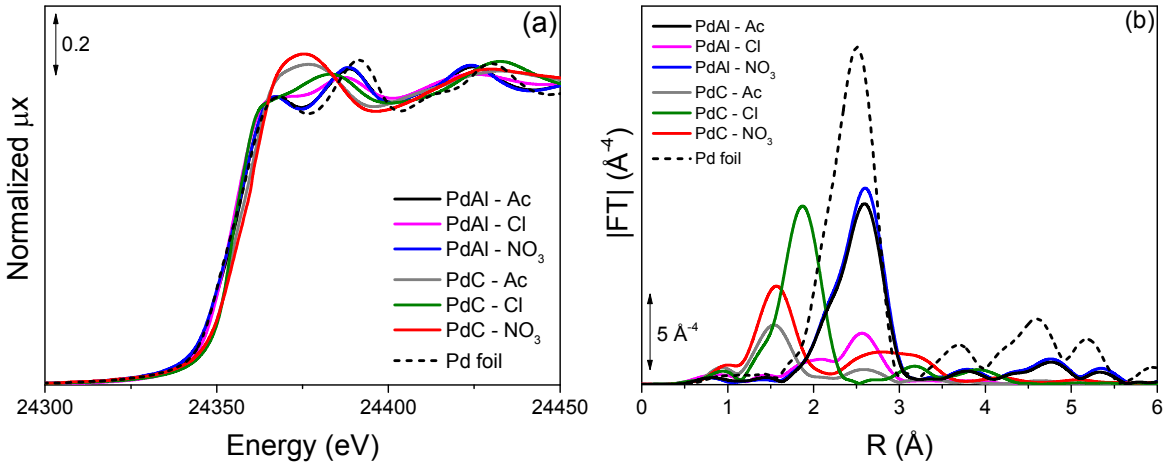

Fig. 6 Normalized XANES spectra (a) and |FT| of the k^3-weighted χ(k) functions (b) of catalysts during reduction in H_2 at 25 ºC.

With increasing the reduction temperature to 200 ºC all XANES spectra (**Fig. 7a**) resemble Pd foil with absorption edges at 24350 eV and the oscillations beyond the edge are flattened respect to foil, indicating different sizes of formed Pd nanoparticles. The PdC-Cl sample display a very subtle shoulder at 24355 eV, which indicates that the reduction process possibly is not completed, but this behavior will be addressed further. The shift in energy observed in the oscillations beyond the edge attributed to PdH_x formation is no longer appreciable once at higher temperatures the palladium hydrides are not stable and are consequently decomposed. The k^3-weighted (phase-uncorrected) |FT| of catalysts during reduction at 200 ºC are shown in **Fig. 7b**. Mainly one peak between 2-3 Å is present in all spectra, related to Pd-Pd distance in Pd metal. The PdC-Cl catalyst also display a shoulder centered at 1.85 Å attributed to Pd-Cl contribution coming from the precursor, which indicates an incomplete decomposition of this precursor at these activation conditions. The formed Pd nanoparticles are smaller than the palladium metal standard, due the absence of the peaks at high R-range. However, it is important to highlight that Pd metal was measured at room temperature while the samples were measured at 200 ºC, which consequently affects the EXAFS signal (Debye-Waller effect) due to thermal motion. This behavior can also be well visualized in the k-space for spectra measured at 200 ºC (**Fig. S3**, ESI†). A clear trend between Pd precursor and intensity of Pd-Pd contribution in |FT| is observed for both supports, with larger nanoparticles observed for the catalysts based on Al_2O_3 in comparison with carbon (better visualized on inset

Physical Chemistry Chemical Physics Accepted Manuscript

View Article Online
DOI: 10.1039/C8CP00517F

Published on 05 April 2018. Downloaded by Freie Universitaet Berlin on 06/04/2018 12:02:04.

of **Fig. 7b**). However, the average size of nanoparticles among all catalysts is as follows: PdC-Cl < PdAl-Cl ≈ PdC-Ac < PdC-NO_3 < PdAl-Ac < PdAl-NO_3. On the other hand, comparing the three precursors it is possible to observed that both classes of catalysts (Pd/Al_2O_3 and Pd/C) behave equally, i.e., the $PdCl_2$ generates smaller nanoparticles than $Pd(OAc)_2$, which in turn generates smaller nanoparticles than $Pd(NO_3)_2$ (inset of **Fig. 7b**).

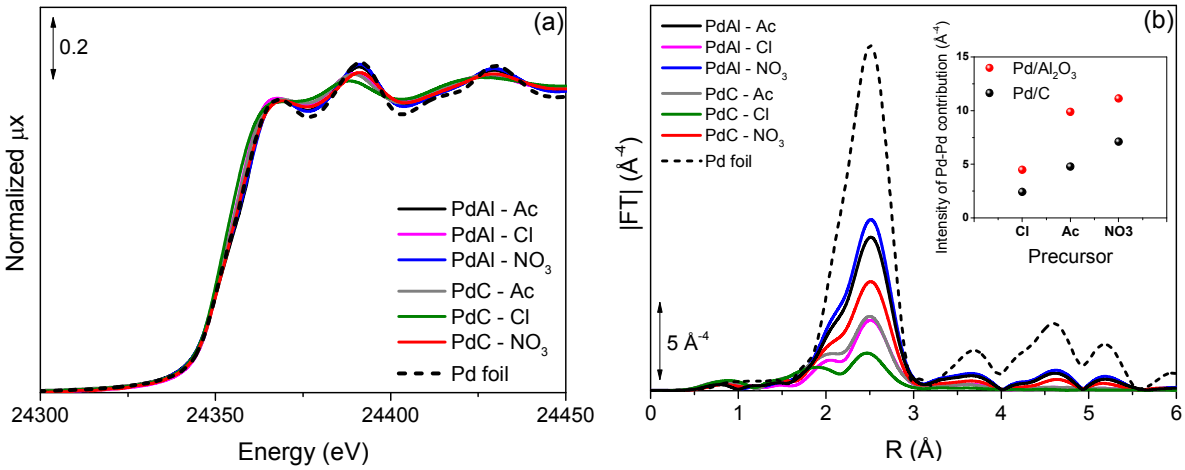

Fig.7 Normalized XANES spectra (a) and |FT| of the k^3-weighted χ(k) functions (b) of catalysts during reduction in H_2 at 200 ºC. The inset in part (b) shows the plot of intensity of |FT| versus type of Pd precursor in Pd/Al_2O_3 and Pd/C catalysts during reduction in H_2 at 200 ºC.

The quantitative results derived from EXAFS data analysis of Pd catalysts during reduction at 200 ºC are shown in **Table 4**. It is known that parameters such as amplitude and Debye-Waller factor can exhibit strong correlation during data analysis[42]. To minimize this problem we have adopt a co-refinement fit of spectra, thus resulting into only one Debye-Waller factor (0.0095 $Å^2$) and photoelectron energy origin correction (ΔE_0 = 2.4 eV) values for all catalysts studied at 200 ºC. The average coordination number obtained for the studied catalysts at 200 ºC varied significantly according to the precursor. As already discussed above, the difficult decomposition of $PdCl_2$ generates catalysts with significantly low average coordination number irrespective to the studied support (4.7 for Pd/Al_2O_3 and 2.3 for Pd/C). These obtained coordination numbers point to the formation of significant clustered Pd species using $PdCl_2$ as precursor. It is worth noticing that despite the presence of remaining Pd-Cl contribution visible

Physical Chemistry Chemical Physics Accepted Manuscript

View Article Online
DOI: 10.1039/C8CP00517F

Published on 05 April 2018. Downloaded by Freie Universitaet Berlin on 06/04/2018 12:02:04.

in |FT|, it is challenging to fit these contributions since a reliable model for this phase is not available. On the other hand, using $Pd(NO_3)_2$ the catalysts presented higher number of neighbors (12 for Pd/Al_2O_3 and 7.6 for Pd/C), achieving bulk size of formed Pd species in the case of former catalyst. Among the examined precursors, the nitrated compound produces Pd nanoparticles with higher CN for Pd-Pd contribution and consequently bigger nanoparticles. The catalyst PdAl-Ac similarly presented considerable Pd-Pd coordination number (CN = 10.7), which can be attributed to large nanoparticles. As expected, the Pd-Pd distance for the investigated catalysts is shorter than in Pd foil (R_{Pd-Pd} = 2.74 Å), equivalent to quantum size effects [43]. In the case of PdC-Cl, the Pd-Pd bond is even shorter than the other catalysts due to substantially small size of Pd clusters. The r-factors explicit the quality of adjusted parameters and it is clear that the catalysts prepared with $PdCl_2$ showed the higher error among their data set, for instance, 0.0746 for PdC-Cl among Pd/C samples, and 0.0198 for PdAl-Cl among Pd/Al_2O_3 samples. This can be explained by the unfitted "tail" visible in |FT| related to the presence remaining ligands of $PdCl_2$ precursor, which is also visible in PdC-Ac. This could result in slightly underestimation of coordination number due to a fraction of Pd atoms involved in Pd-Cl bonding. The other catalysts presented very small errors, confirming the quality of the fit. The fits in both q-space and R-space are included in the ESI† (**Fig. S4** and **Fig. S5**, respectively).

Table 4 Summary of optimized parameters by fitting EXAFS data of catalysts at 200 ºC in H_2[a]

Sample	CN	Path	R (Å)	σ^2 (Å^2)	ΔE_0 (eV)	r-factor
PdAl-Ac	10.7 ± 0.4	Pd-Pd	2.731 ± 0.002	0.0095 ± 0.0002	2.4 ± 0.4	0.0024
PdAl-Cl	4.7 ± 0.2		2.735 ± 0.003			0.0198
PdAl-NO_3	12.0 ± 0.4		2.733 ± 0.002			0.0026
PdC-Ac	4.9 ± 0.3		2.733 ± 0.003			0.0123
PdC-Cl[b]	2.3 ± 0.2	Pd-Pd	2.726 ± 0.008			0.0746
PdC-NO_3	7.6 ± 0.4		2.729 ± 0.004			0.0007

[a]A simultaneous fit of the spectra was adopted, fixing the σ^2 and ΔE_0 values; the fits were performed on the first coordination shell (ΔR = 2.2-3.0 Å) over FT of the k^3-weighted $\chi(k)$ functions performed in the Δk = 2.3-13.7 Å^{-1} interval, resulting into a number of independent parameters of $2\Delta R\Delta k/\pi$ = 38.8. Non optimized parameters are recognizable by the absence of the corresponding error bar. [b]ΔR = 1.4-3.0 Å.

As a way of evaluating possible nanoparticles growth (or remaining ligands decomposition in the case of PdC-Cl catalyst) during cooling process (200 ºC → 25 ºC) under H_2

Physical Chemistry Chemical Physics Accepted Manuscript

View Article Online
DOI: 10.1039/C8CP00517F

Published on 05 April 2018. Downloaded by Freie Universitaet Berlin on 06/04/2018 12:02:04.

flow and also to validate the co-refinement fitting performed at higher temperature, the EXAFS spectra have been measured at 25 ºC (state in which the catalysts will be used). The quantitative results derived from EXAFS data analysis are shown in **Table S2** (ESI†). As for the catalysts measured at 200 ºC, here we have also made a co-refinement fitting of spectra resulting into only one Debye-Waller factor (0.0082 $Å^2$) and photoelectron energy origin correction (ΔE_0, 2.9 eV) for the whole set of data measured in these conditions. With exception of Pd-Pd distance, there are only small differences between the samples after reduction (25 ºC) and during reduction at 200 ºC, the average coordination numbers and the r-factors slightly deviate from the spectra measured at 200 ºC. It is worth noticing that we cannot rule out that the catalysts continue to reduce during the cooling process in PdC-Cl and PdAl-Cl catalysts. The biggest differences are attributed to Debye-Waller factor (which in this case is smaller at room temperature than at 200 ºC due to decrease in temperature) and Pd-Pd distances. With the decrease in temperature, the distances Pd-Pd increase due to the insertion of H in Pd lattice in the formation of PdH_x. However, the distances seem to be different for each catalyst, and it is possible to correlate the different Pd-Pd distances to the different coordination numbers obtained, thus the shorter is the distance, the smaller the coordination number is. This behavior can be explained by the fact that when the particle is bigger, there are a higher number of interior octahedral sites available for hydrogen incorporation.[19]

CONCLUSIONS

In this work we followed by *in situ* XAS the activation process of 7 wt% Pd-based catalysts (Pd supported on Al_2O_3 and activated carbon) using three different metal precursors: $Pd(OAc)_2$, $PdCl_2$ and $Pd(NO_3)_2$. We find that the nature of Pd precursor and activation procedure (e.g. calcination process) influence metal dispersion and average particle size. First, the easiest decomposition of $Pd(NO_3)_2$ respect to other precursors always gives rise to PdO formation, even during the impregnation step, and consequently larger nanoparticles are formed at the end of activation process. Similarly, $Pd(OAc)_2$ follows a very similar activation path through PdO species, but its formation needs slightly higher temperatures. Finally, the activation of the catalysts in which $PdCl_2$ was used as precursor goes by a different way. Al_2O_3-based catalysts pass through an intermediate phase ($PdO_{0.75}Cl_{0.25}$) during calcination in air, which is decomposed

Physical Chemistry Chemical Physics Accepted Manuscript

View Article Online
DOI: 10.1039/C8CP00517F

during reduction. On the other hand, Cl-species were identified in the carbon-based sample even after reduction. Moreover, according to EXAFS amplitude decreasing, we found that $PdCl_2$ generates smaller nanoparticles than $Pd(OAc)_2$, which in turn generates smaller nanoparticles than $Pd(NO_3)_2$, independent of used support. The use of *in situ* XAS has allowed tracking the activation processes of a series of Pd supported catalysts and could be useful for the selection of the right Pd precursor during synthesis of Pd based catalysts.

CONFLICTS OF INTEREST

There are no conflicts to declare.

ACKNOWLEDGEMENTS

The authors thank the Spanish Ministry of Economy and Competitiveness through MAT2015-71842-P (MINECO/FEDER) and SEV-2016-0683 projects for the financial support. We gratefully acknowledge ALBA synchrotron for allocating beamtime (proposal 2015091414) and the CLÆSS beamline staff for their help and technical support during our experiment. C.W. Lopes (Science without Frontiers - Process no. 13191/13-6) thanks CAPES for a predoctoral fellowship. J.L. Cerrillo wishes to thank MINECO for the Severo Ochoa contract for PhD formation (SVP-2014-068600).

REFERENCES

1. X. Chen, X. Huo, J. Liu, Y. Wang, C. J. Werth and T. J. Strathmann, *Chemical Engineering Journal*, 2017, **313**, 745-752.
2. C. Lu, M. Wang, Z. Feng, Y. Qi, F. Feng, L. Ma, Q. Zhang and X. Li, *Catal. Sci. Technol.*, 2017, **7**, 1581-1589.
3. O. S. G. P. Soares, C. M. A. S. Freitas, A. M. Fonseca, J. J. M. Órfão, M. F. R. Pereira and I. C. Neves, *Chemical Engineering Journal*, 2016, **291**, 199-205.
4. P. Yaseneva, C. F. Marti, E. Palomares, X. Fan, T. Morgan, P. S. Perez, M. Ronning, F. Huang, T. Yuranova, L. Kiwi-Minsker, S. Derrouiche and A. A. Lapkin, *Chemical Engineering Journal*, 2014, **248**, 230-241.
5. P. A. Kalmykov and M. V. Klyuev, *Petroleum Chemistry*, 2016, **56**, 27-32.
6. A. B. Gaspar and L. C. Dieguez, *Applied Catalysis A: General*, 2000, **201**, 241-251.

Published on 05 April 2018. Downloaded by Freie Universitaet Berlin on 06/04/2018 12:02:04.
Physical Chemistry Chemical Physics Accepted Manuscript

View Article Online
DOI: 10.1039/C8CP00517F

Published on 05 April 2018. Downloaded by Freie Universitaet Berlin on 06/04/2018 12:02:04.

7. A. K. Khudorozhkov, I. A. Chetyrin, A. V. Bukhtiyarov, I. P. Prosvirin and V. I. Bukhtiyarov, *Topics in Catalysis*, 2017, **60**, 190-197.
8. A. A. Vedyagin, A. M. Volodin, R. M. Kenzhin, V. O. Stoyanovskii, V. A. Rogov, D. A. Medvedev and I. V. Mishakov, *Journal of Thermal Analysis and Calorimetry*, 2017, DOI: 10.1007/s10973-017-6530-y.
9. C. Wang, F. Yang, W. Yang, L. Ren, Y. Zhang, X. Jia, L. Zhang and Y. Li, *RSC Advances*, 2015, **5**, 27526-27532.
10. F. Di Natale, M. Orefice, F. La Motta, A. Erto and A. Lancia, *Separation and Purification Technology*, 2017, **174**, 183-193.
11. M. L. Toebes, J. A. van Dillen and K. P. de Jong, *Journal of Molecular Catalysis A: Chemical*, 2001, **173**, 75-98.
12. P. Munnik, P. E. de Jongh and K. P. de Jong, *Chem Rev*, 2015, **115**, 6687-6718.
13. J. A. Moulijn, A. E. van Diepen and F. Kapteijn, *Applied Catalysis A: General*, 2001, **212**, 3-16.
14. G. Agostini, C. Lamberti, R. Pellegrini, G. Leofanti, F. Giannici, A. Longo and E. Groppo, *ACS Catalysis*, 2013, **4**, 187-194.
15. S. J. Cho and S. K. Kang, *The Journal of Physical Chemistry B*, 2000, **104**, 8124-8128.
16. M. Harada and Y. Inada, *Langmuir*, 2009, **25**, 6049-6061.
17. J. Singh, C. Lamberti and J. A. van Bokhoven, *Chem Soc Rev*, 2010, **39**, 4754-4766.
18. D. C. Koningsberger and R. Prins, *X-Ray Absorption: Principles, Applications, Techniques of EXAFS, SEXAFS and XANES*, Wiley, 1988.
19. J. Wang, Q. Wang, X. Jiang, Z. Liu, W. Yang and A. I. Frenkel, *The Journal of Physical Chemistry C*, 2015, **119**, 854-861.
20. G. Agostini, R. Pellegrini, G. Leofanti, L. Bertinetti, S. Bertarione, E. Groppo, A. Zecchina and C. Lamberti, *The Journal of Physical Chemistry C*, 2009, **113**, 10485-10492.
21. A. I. Frenkel, C. W. Hills and R. G. Nuzzo, *The Journal of Physical Chemistry B*, 2001, **105**, 12689-12703.
22. A. I. Frenkel, *J Synchrotron Radiat*, 1999, **6**, 293-295.
23. G. Agostini, A. Piovano, L. Bertinetti, R. Pellegrini, G. Leofanti, E. Groppo and C. Lamberti, *The Journal of Physical Chemistry C*, 2014, **118**, 4085-4094.
24. S. Brunauer, P. H. Emmett and E. Teller, *Journal of the American Chemical Society*, 1938, **60**, 309-319.
25. K. S. W. Sing, F. Rouquerol, P. Llewellyn and J. Rouquerol, in *Adsorption by Powders and Porous Solids*, 2014, DOI: 10.1016/b978-0-08-097035-6.00009-7, pp. 303-320.
26. K. S. W. Sing, F. Rouquerol, J. Rouquerol and P. Llewellyn, in *Adsorption by Powders and Porous Solids*, 2014, DOI: 10.1016/b978-0-08-097035-6.00008-5, pp. 269-302.
27. L. Simonelli, C. Marini, W. Olszewski, M. ��vila P��rez, N. Ramanan, G. Guilera, V. Cuartero, K. Klementiev and N. L. Saini, *Cogent Physics*, 2016, **3**.
28. G. Guilera, F. Rey, J. Hernández-Fenollosa and J. J. Cortés-Vergaz, *Journal of Physics: Conference Series*, 2013, **430**.
29. B. Ravel and M. Newville, *J Synchrotron Radiat*, 2005, **12**, 537-541.
30. Y. Yazawa, H. Yoshida, N. Takagi, S.-i. Komai, A. Satsuma and T. Hattori, *Applied Catalysis B: Environmental*, 1998, **19**, 261-266.
31. M. Thommes, K. Kaneko, A. V. Neimark, J. P. Olivier, F. Rodriguez-Reinoso, J. Rouquerol and K. S. W. Sing, *Pure and Applied Chemistry*, 2015, **87**.

Physical Chemistry Chemical Physics Accepted Manuscript

View Article Online
DOI: 10.1039/C8CP00517F

32. C.-M. Lin, T.-L. Hung, Y.-H. Huang, K.-T. Wu, M.-T. Tang, C.-H. Lee, C. T. Chen and Y. Y. Chen, *Physical Review B*, 2007, **75**.
33. A. Frenkel, *Zeitschrift für Kristallographie - Crystalline Materials*, 2007, **222**.
34. M. Fernández-García, *Catalysis Reviews*, 2002, **44**, 59-121.
35. G. Agostini, E. Groppo, A. Piovano, R. Pellegrini, G. Leofanti and C. Lamberti, *Langmuir*, 2010, **26**, 11204-11211.
36. S.-J. Kim, S. Lemaux, G. Demazeau, J.-Y. Kim and J.-H. Choy, *Journal of Materials Chemistry*, 2002, **12**, 995-1000.
37. E. Groppo, W. Liu, O. Zavorotynska, G. Agostini, G. Spoto, S. Bordiga, C. Lamberti and A. Zecchina, *Chemistry of Materials*, 2010, **22**, 2297-2308.
38. J. Góralski, B. Szczepaniak, J. Grams, W. Maniukiewicz and T. Paryjczak, *Polish Journal of Chemical Technology*, 2007, **9**.
39. G. Agostini, E. Groppo, S. Bordiga, A. Zecchina, C. Prestipino, F. D'Acapito, E. van Kimmenade, P. C. Thüne, J. W. Niemantsverdriet and C. Lamberti, *The Journal of Physical Chemistry C*, 2007, **111**, 16437-16444.
40. W.-J. Shen, Y. Ichihashi, H. Ando, M. Okumura, M. Haruta and Y. Matsumura, *Applied Catalysis A: General*, 2001, **217**, 165-172.
41. A. L. Bugaev, A. A. Guda, A. Lazzarini, K. A. Lomachenko, E. Groppo, R. Pellegrini, A. Piovano, H. Emerich, A. V. Soldatov, L. A. Bugaev, V. P. Dmitriev, J. A. van Bokhoven and C. Lamberti, *Catalysis Today*, 2017, **283**, 119-126.
42. M. S. Nashner, A. I. Frenkel, D. L. Adler, J. R. Shapley and R. G. Nuzzo, *Journal of the American Chemical Society*, 1997, **119**, 7760-7771.
43. J. H. Kang, L. D. Menard, R. G. Nuzzo and A. I. Frenkel, *J Am Chem Soc*, 2006, **128**, 12068-12069.

Published on 05 April 2018. Downloaded by Freie Universitaet Berlin on 06/04/2018 12:02:04.

Physical Chemistry Chemical Physics Accepted Manuscript